Electronic Supplementary Material (ESI) for Soft Matter

Phase Behaviors and Janus Hierarchical Supramolecular Structures Based on Asymmetric Tapered Bisamide

Hao-Jan Sun,[a] *Chien-Lung Wang,*[a,b] *I-Fan Hsieh,*[a] *Chih-Hao Hsu,*[a] *Ryan M. Van Horn,*[a] *Chi-Chun Tsai,*[a] *Kwang-Un Jeong,*[c] *Bernard Lotz,*[d] *and Stephen Z.D. Cheng**[a]

[a]Department of Polymer Science, College of Polymer Science and Polymer Engineering, E-mail:scheng@uakron.edu

The University of Akron, Akron, OH, 44325, USA

[b]Department of Applied Chemistry, National Chiao Tung University, 1001 Ta Hsueh Road, Hsinchu, Taiwan 300, ROC

[c]Polymer Bin Fusion Research Center, Department of Polymer Nano-Science and Technology, Chonbuk National University, Jeonju, Jeonbuk 561-756, Korea

[d]Institut Charles Sadron, 23, Rue du Loess, Strasbourg 67034, France

1. Synthesis route and molecule identification of $C_{22}PhBAEO_3$:

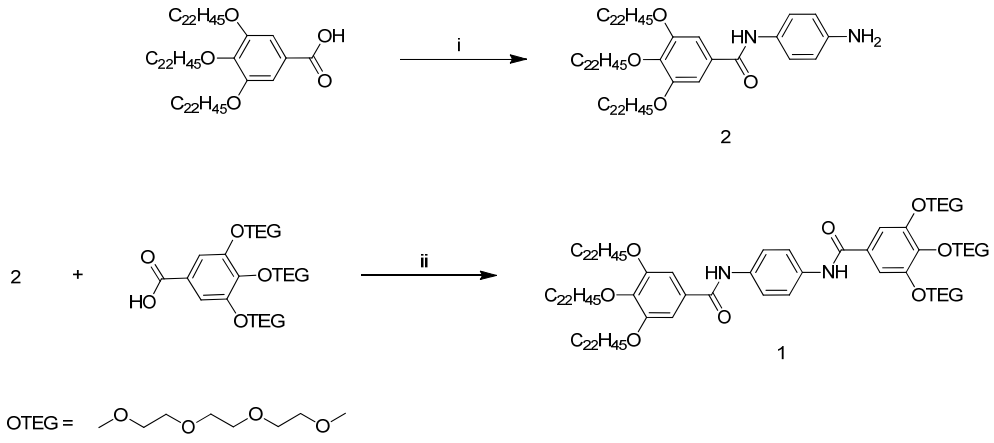

Figure S1: Synthetic route of $C_{22}PhBAEO_3$ (**1**). Reagents and conditions: (i) 1,4-Phenylenediamine, N,N'-Diisopropylcarbodiimide (DIPC), 4-(dimethylamino) pyridinium toluene-p-sulfonate (DPTS), THF/CH_2Cl_2 = 1/4, 25 °C; (ii) N-(3-Dimethylaminopropyl)-N'-ethylcarbodiimide hydrochloride (EDC•HCl), 1-hydroxybenzotriazole (HOBT), CH_2Cl_2, 25 °C.

THF and methanol was purchased from Aldrich as reagent grade and used as received. Anhydrous grade CH_2Cl_2 was purchased from Acros. All other reagents were purchased as reagent grade and used without further purification unless otherwise noted. 3,4,5-tris-docosoxybenzoic acid and methyl 3,4,5-tris(2-(2-(2-hydroxyethoxy)ethoxy)-ethoxy)benzoic acid were synthesized according to the literature[1,2].

Synthesis of $C_{22}NH_2$ (2).

1,4-Phenylenediamine (292 mg, 2.70mmol), 3,4,5-tris-docosoxy benzoic acid (300mg, 0.27 mmol), and DPTS (4-dimethylamino-pyridinium-4-toluene sulfonate, 10 mg, 0.03 mmol) was dissolved in 50mL THF/CH_2Cl_2 mixture with ratio THF/CH_2Cl_2 = 1/4 (v/v) and cooled to 0 ^oC. DIPC (diisopropylcarbo- diimide, 500mg 3.96 mmol) was then added into the mixture and the solution was stirred for one day. After 24 hours, 50 mL H_2O was added into the solution, and the solution was brought to room temperature and stirred for another 10 minutes. The aqueous phase was extracted with CH_2Cl_2 (3 x 50 mL), and the combined organic phase was washed with brine (50 mL), then dried ($MgSO_4$), and concentrated to give brown solid. The crude product was re-precipitated out from MeOH and subjected to column chromatography (SiO_2, CH_2Cl_2/THF = 20/1 (v/v)) to remove double substituted bisamide and obtain compound **2** as white solid. After chromatography, products were re-precipitated out from MeOH. Yield: 260 mg, 81%. ^1H NMR (300 MHz, CDCl3): δ(ppm) 7.52 (s, 1H), 7.39 (d, J = 8.7 Hz, 2H), 7.03 (s, 2H), 6.71 (d, J = 8.7 Hz, 2H), 3.97-4.06 (m, 6H), 3.64 (brs, 2H), 1.73-1.85 (m, 6H), 1.43-1.48 (m, 6H), 1.27 (brs, 108H), 0.89 (t, J = 6.9 Hz, 9H). ^{13}C NMR (75 MHz, CDCl3): δ(ppm) 165.7, 153.4, 143.7, 141.4, 130.4, 129.5, 122.4, 115.7, 105.9, 73.7, 69.6, 32.1, 30.5, 30.0, 29.9, 29.9, 29.9, 29.8, 29.6, 29.6, 26.3, 22.9, 14.3. (Figure S2)

Synthesis of $C_{22}EO_3$bisamide ($C_{22}PhBAEO_3$, 1).

2 (100 mg, 0.08 mmol), methyl 3,4,5-tris(2-(2-(2-hydroxyethoxy)ethoxy)-ethoxy)benzoic acid (104 mg, 0.17 mmol), N-(3-Dimethylaminopropyl)-N'-

ethylcarbodiimide hydrochloride (30 mg, 0.16 mmol), and 1-hydroxybenzotriazole (25 mg, 0.18 mmol) weredissolved in 5 mL CH_2Cl_2 and stirred at room temperature for 24 hours. 15 mL CH_2Cl_2 was added into the solution, and the solution was washed with H_2O (10 mL) and brine (10 mL). The organic phase was dried ($MgSO_4$) and concentrated to give crude product. The crude product was re-precipitated out from MeOH and subjected to column chromatography (SiO_2, CH_2Cl_2/THF = 1/1 (v/v)) to obtain C_{22}PhBAEO_3bisamide (**1**) as light yellow solid. Yield: 120 mg, 85%.^{1}H NMR (300 MHz, $CDCl_3$): δ(ppm) 8.35 (s, 1H), 7.78 (s, 1H), 7.70 (d, *J* = 9 Hz, 2H), 7.64 (d, *J* = 9 Hz, 2H), 7.23 (s, 2H), 7.07 (s, 2H), 4.22-4.25 (m, 6H), 4.00-4.07 (m, 6H), 3.85 (t, *J* = 5.1 Hz, 4H), 3.81 (t, *J* = 4.8 Hz, 2H), 3.63-3.74 (m, 18H), 3.51-3.57 (m, 6H), 3.38 (s, 3H), 3.34 (s, 6H), 1.74-1.86 (m, 6H), 1.46-1.49 (m, 6H), 1.27 (brs, 108H), 0.89 (t, *J* = 6.9 Hz, 9H). ^{13}C NMR (75 MHz, $CDCl_3$): δ(ppm) 165.8, 165.6, 153.4, 152.7, 142.0, 141.6, 135.1, 134.6, 130.3, 130.1, 121.3, 121.0, 108.0, 106.0, 73.8, 72.6, 72.1, 72.1, 70.9, 70.8, 70.7, 70.6, 70.0, 69.6, 69.4, 59.2, 59.1, 32.1, 30.5, 30.0, 29.9, 29.9, 29.8, 29.6, 29.6, 26.3, 22.9, 14.3; MALDI–TOF mass: calcd. for $C_{83}H_{42}N_2NaO_{17}$ $[M + Na]^+$: *m/z* = 1798.4; found $[M + Na]^+$: *m/z* = 1798.9 (Figure S3)

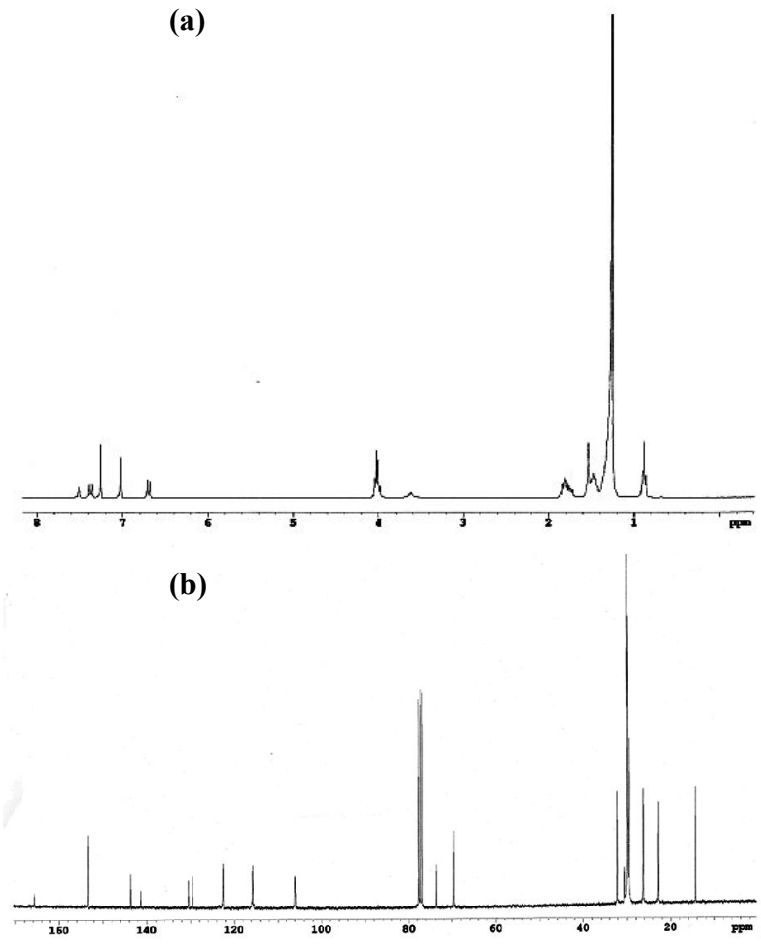

Figure S2.(a) ^{1}H NMR spectrum, and (b) ^{13}C NMR spectrum of **2**.

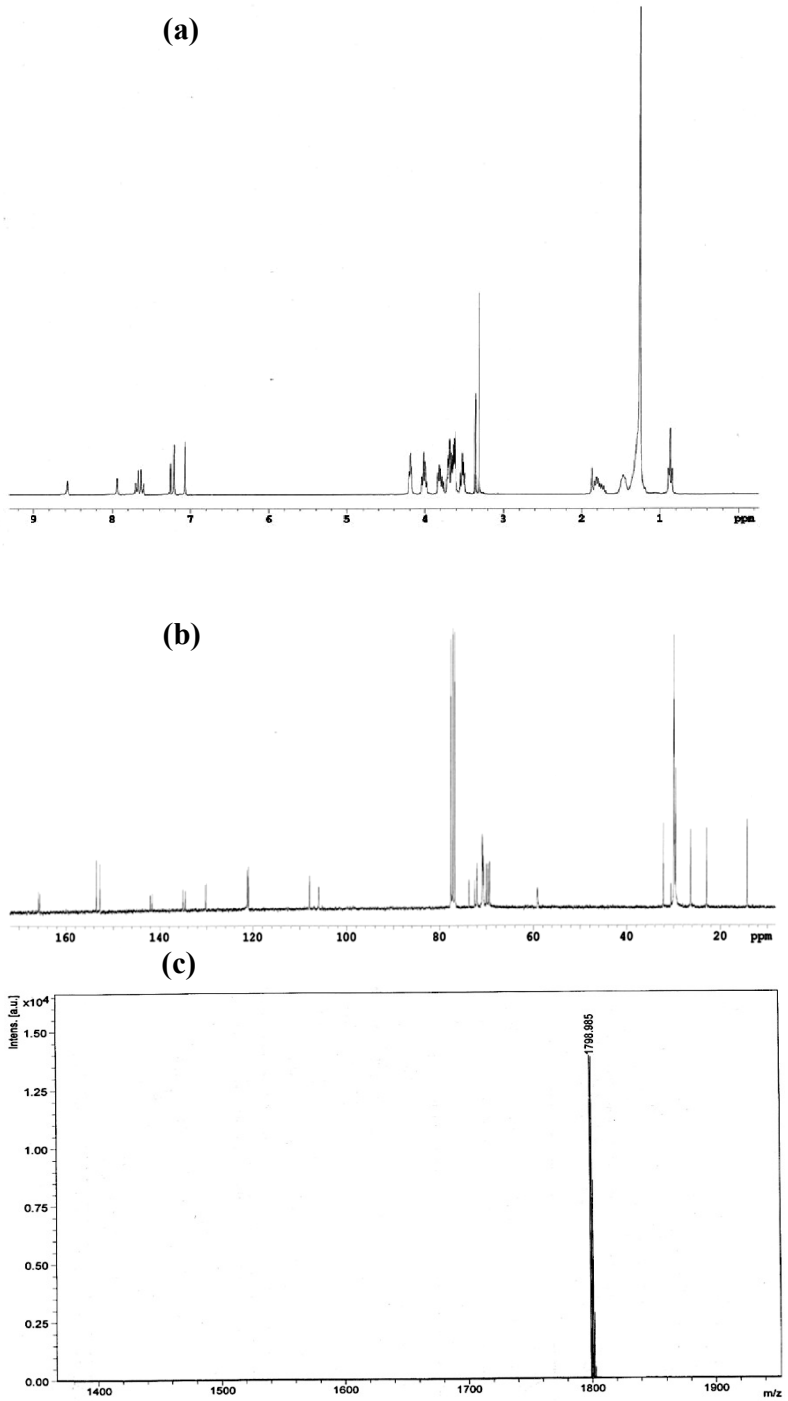

Figure S3.(a) ^{1}H NMR spectrum, (b) ^{13}C NMR spectrum, and (c) MALDI-TOF mass spectrum of **C_{22}PhBAEO_3bisamide (1)**.

2. FTIR analysisof $C_{22}PhBAEO_3$:

Figure S4 shows the FTIR measurements of $C_{22}PhBAEO_3$ at various temperatures. The sample was heated to above 160 °C prior to the measurements to release any thermal history, and the cooling scans at different temperatures were recorded. The H-bonding sensitive bands are at wavenumber 3300 cm^{-1} (H-bonded N-H stretching band, ν_{N-H}) and 1648 cm^{-1} (amide I). The observation of these two bands in the low temperature patterns indicates almost all N-H groups are associated with the C=O groups via H-bonds. Upon heating, the H-bonded ν_{N-H} band becomes weaker and shifted toward higher frequencies (3441 cm^{-1}, free, non-bonded N-H stretching band) showing that a portion of H-bonding dissociated when the temperature is close to the vicinity of the isotropization temperature. This experiment showed that the inter-molecular H-bonding contributed to the formation of supramolecular columnar structures in the three ordered phases found in the $C_{22}PhBAEO_3$ system. Other bands observed in the FTIR diagram can also help us to determine the conformations and/or the molecular interactions. For example, the bands related to rigid amide core can be found at 1608, 1582, 1527, and 1493 cm^{-1}. The bands attributed to the aliphatic tails are located at 2957, 2921, 2873, 2851, 1468, 1382, and 720 cm^{-1}. The bands in the ranges of 2846 – 2850 cm^{-1} and 2916 – 2920 cm^{-1} correspond to the asymmetric stretching (ν_{as}) and symmetric stretching (ν_s) of the CH_2 groups, respectively. Also, the gauche conformations of the alkyl tails can be probed according to the absence of equally spaced CH_2 wagging twisting progression bands between 1170 and 1350 cm^{-1}, which is characteristic for the all trans conformation of alkyl chains.[3,4] More detailed FTIR data analysis can be found in previous publications.[2,5,6]

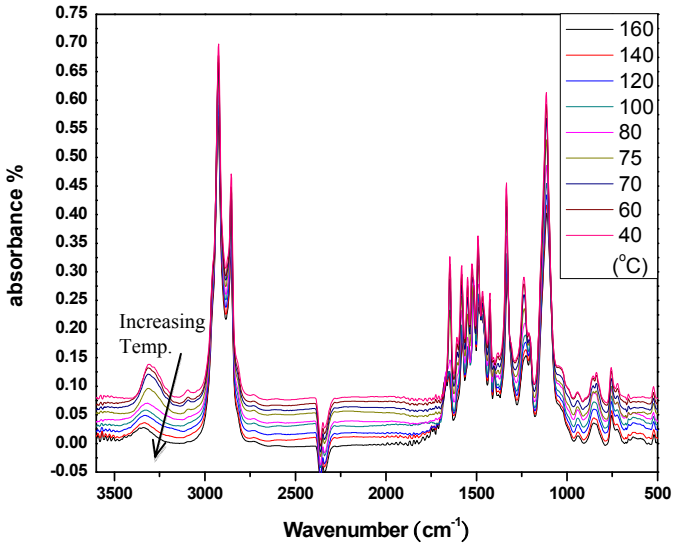

Figure S4.FTIR measurements of C_{22}PhBAEO_3 during cooling.

3. Thermogravimetric analysis (TGA):

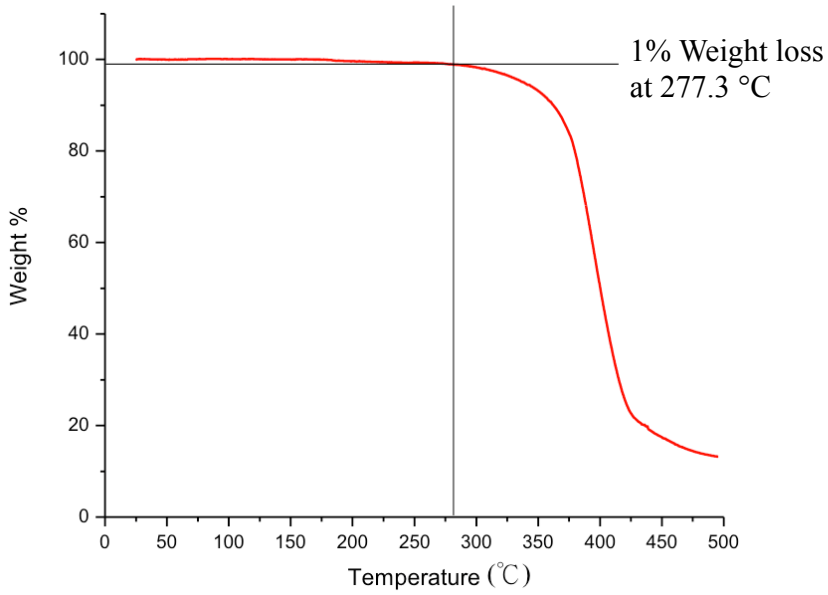

Figure S5.TGA measurements of C_{22}PhBAEO_3 under N_2 atmosphere

Figure S5 shows the TGA measurement result of C_{22}PhBAEO_3bisamide. The compound showed 1% weight loss at around 277 °C. The result indicates the compound is thermally stable even at isotropization temperature (104°C) and both *crystal I* and *crystal II* ordered phases are stable under ordinary operation temperatures.

4. Supporting DSC measurements:

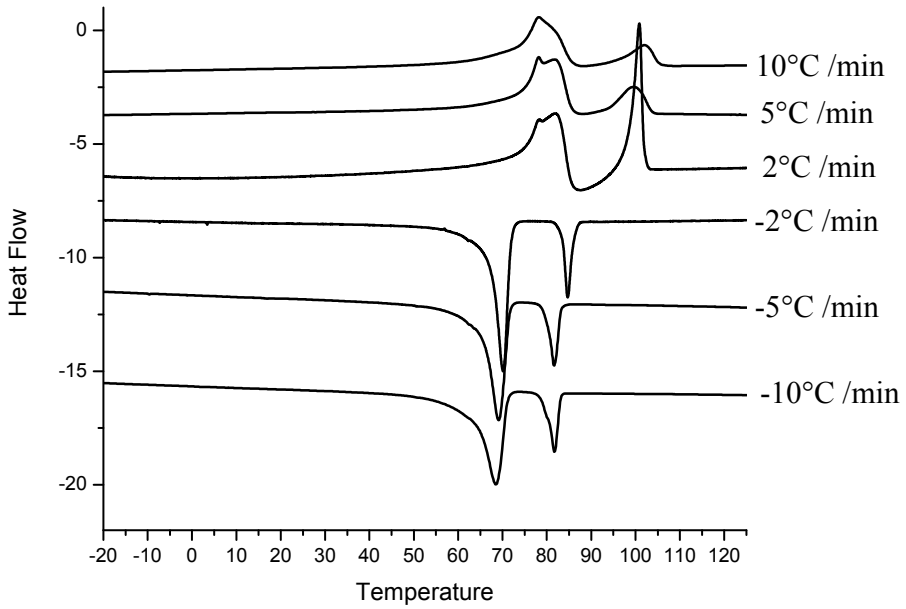

Figure S6.DSC measurements of $C_{22}PhBAEO_3$ at different heating and cooling rate as indicated.

The DSC measurements of $C_{22}PhBAEO_3$at different scan rates were shown in Figure S6. At the slowest heating rate (2°C/min), it can be observed that an exothermic peak represented the rearrangement process of alkyl tails and aromatic core columns appeared immediately after the melting of less ordered alkyl tail crystals formed in *crystal I* phase. The peak indicated the phase transition from *col.* phase to *crystal II* phase. Two overlapped peaks attributed to the melting of *crystal I* phase were observed between 72 °C to 80 °C, indicating two slightly different melting temperatures existed within the phase. We speculate that this observation is from the melting of one crystal

form but with two distinct metastabilities such as two different crystallite sizes within the crystalline hydrophobic domain.

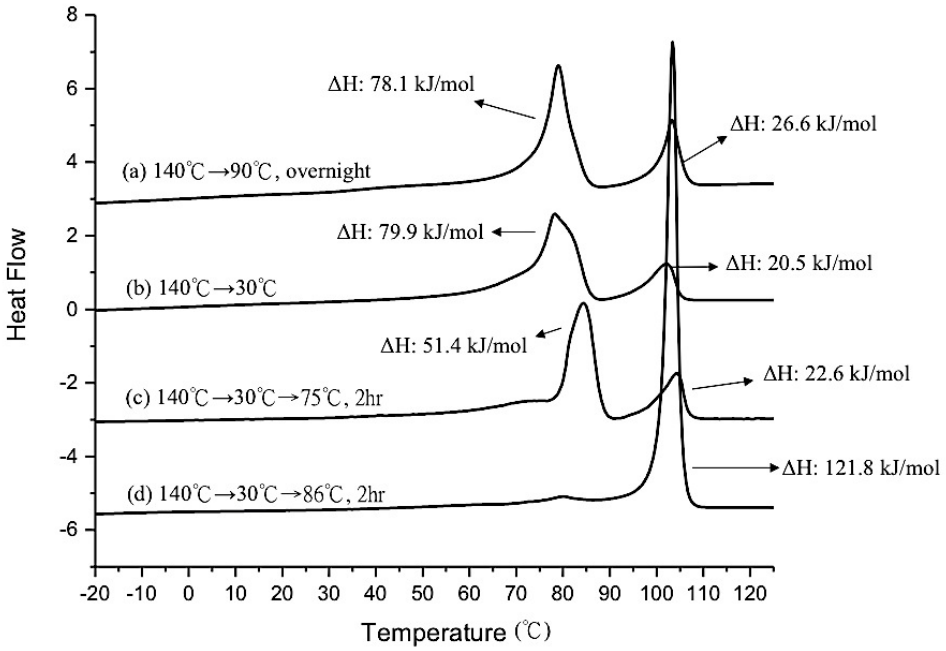

Figure S7.DSC heating measurements of $C_{22}PhBAEO_3$ after different thermal treatments as indicated. The scan rate is 10 °C/min.

DSC Diagrams of samples prepared through various heat treatments are shown in Figure S7. In pattern (a), the sample was annealed at 90°C which is below the melting temperature of *crystal II* phase but above the formation temperature of *col.* phase. The molecules did not enter the *crystal II* phase even when annealed overnight, while this transition required less than two hours to complete if the system entered *col.* phase first as shown in pattern (d). It thus clearly indicated that the *col.* phase is the precursor of the most stable *crystal II* phase. The lateral packing of supramolecular columns and the crystallinity evolution of the alkyl tails have to be based on the phase-separated *col.* phase. Pattern (b) and (c) show the heating diagrams of sample directly cooled down to

room temperature from the isotropic state and annealed at 75 °C for two hours, respectively. The two patterns are similar except a slight shift of the melting of alkyl tails toward higher temperature after annealing. This result is consistent with the heating pattern shown in Figure S6 where two melting peaks corresponding to two different alkyl tail crystal sizes were observed.

5. Supporting 1D WAXD patterns of *crystal II* phase:

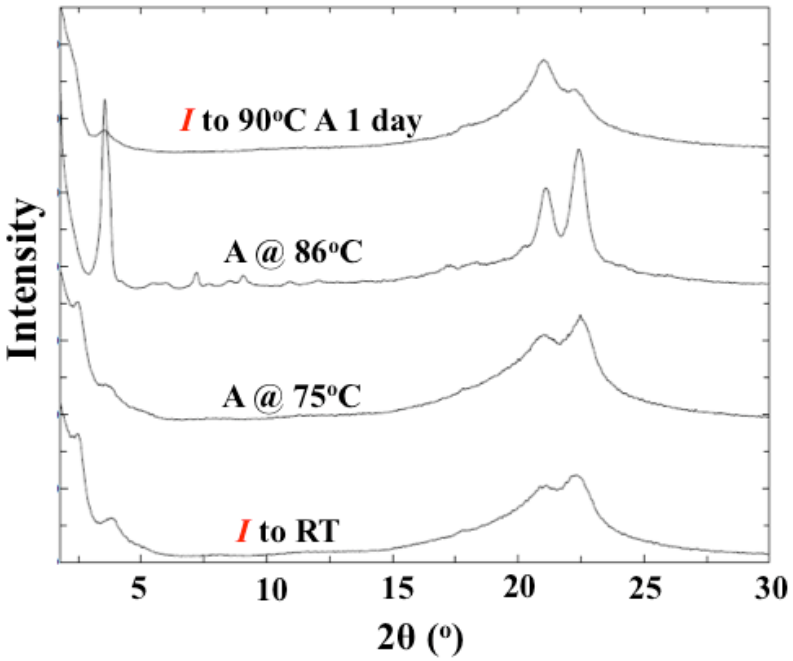

Figure S8.1D WAXD patterns of samples from different heat treatments prior tomeasurement at RT.

The 1D WAXD patterns shown in Figure S8 indicate that the *col.* phase is the precursor of the high order *crystal II* phase. It can be observed that the molecules did not enter the *crystal II* phase when annealed at 90 °C for one day although this temperature is already lower than the *crystal II*formationtemperature (top pattern). On the other hand, this transition can be complete within two hours under *col.*phase (second pattern from top).

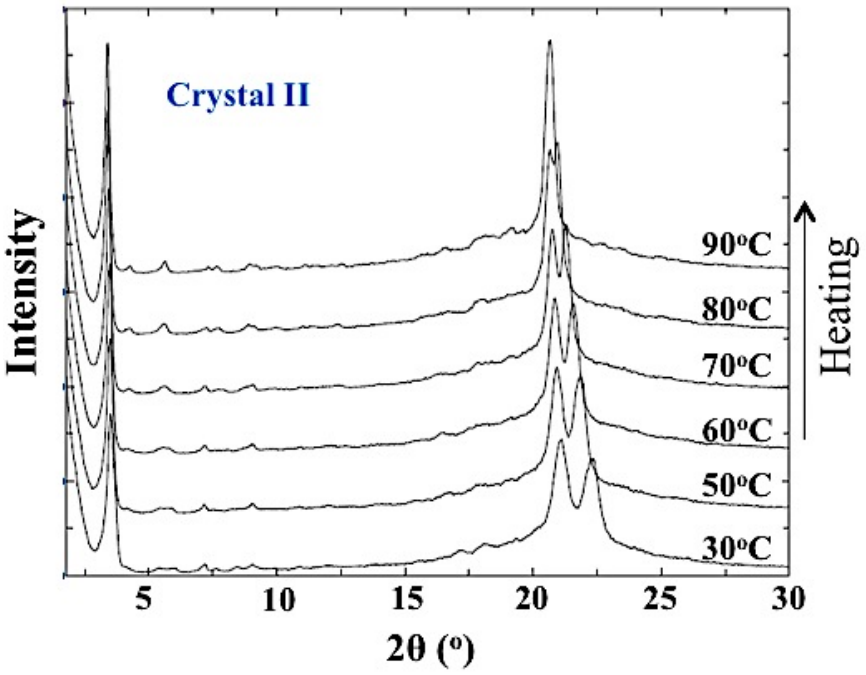

Figure S9.1D WAXD patterns of *crystal II* phase collected at indicated temperatures.

From the 1D WAXD patterns collected at various temperatures within the *crystal II* phase, the alkyl tail crystals were found to gradually enter a "rotator phase" during heating in which the diffractions of (110) and (200) merged together at elevated temperature to form a hexagonal like packing starting at around 82 °C.[7-9] The alkyl crystals returned to normal orthorhombic packing at room temperature.

Transition from crystal phase to rotator phase is a first order transition that occurs in *n*-alkanes with chain length under 40 carbons. The molecules enter the rotator phase on heating at elevated temperatures close to the melting temperature.[7-9]In the rotator phase, the molecules can rotate locally within the crystal lattice along the chain axis. That is, the molecules lose the bond orientation order but keep molecular orientation and positional

order. It is an entropy-driven transition. Therefore, we don't see a transition peak in the DSC diagram during the process since the DSC only detects enthalpic phase transitions.

6. ED fiber pattern of *crystal II* and simulated XRD fiber pattern of PE crystal:

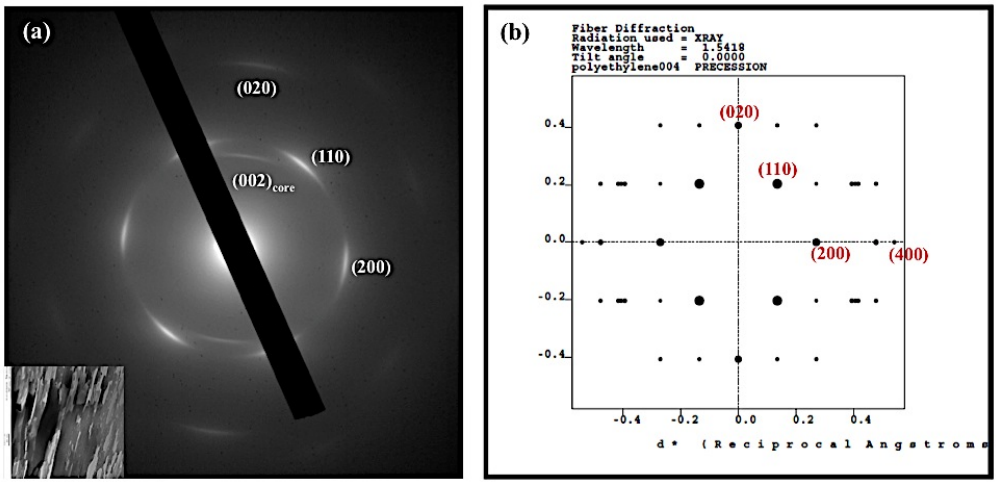

Figure S10.(a) ED fiber pattern of $C_{22}PhBAEO_3$ *crystal II* phase. Sample sheared at 75 °C during cooling then annealed at 87 °C for 2 hours. (b) Simulated polyethylene fiber pattern with b-axis being the fiber axis.

Figure S10a shows the fiber pattern obtained from *crystal II* phase after mechanical shearing and annealing process. One pair of arcs appeared on the meridian attributed to the (002) diffraction of the aromatic core packing was indicated. The remaining arcs belong to the fiber diffractions of alkyl tail crystals. Compared with the computer simulated fiber diffraction result of polyethylene showed in Figure S10b, it is clear that the alkyl tails packed within the hydrophobic layer with the *b*-axis parallel to the column axis.

7. Proposed supramolecular disc formation mechanism:

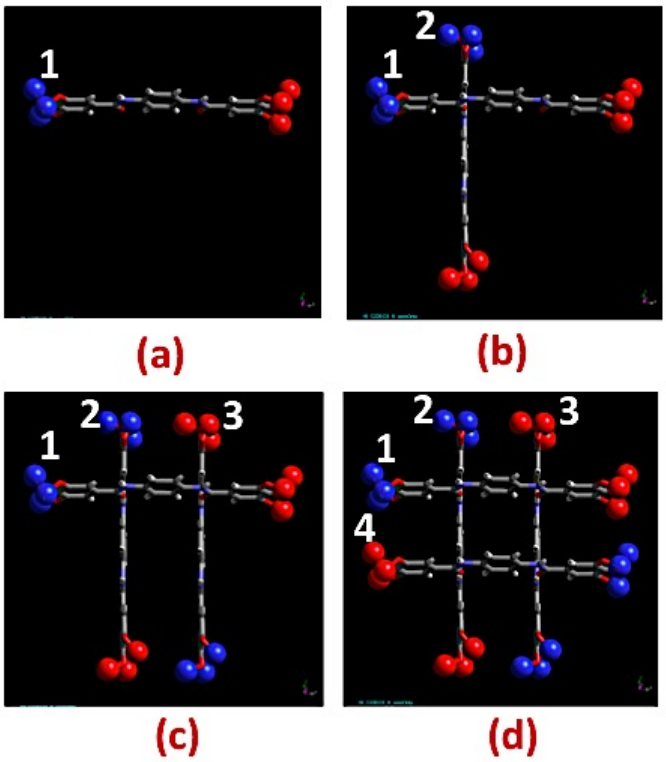

Figure S11. Step by step formation mechanism of C_{22}PhBAEO_3supramolecular disc.

Figure S11 shows the Janus twin dendron molecules self-assembled into phase-separated ellipsoid disc as the first level of hierarchical structure in the asymmetric amphiphile system. The four cross points of the aromatic cores are connected by H-bonding. The reason of forming this disc structure is two-fold. First, this packing can mediate the unbalanced stress stored in higher level of hierarchical structures, so it is physically more favored. The second reason relates to the H-bonding formation process. When the third and forth molecule approach and form H-bonds, the situation showed in Figures S11c and S11d is most possible because the distance between two H-bonded

molecules (1 and 3, 0.49 nm) is shorter than the two face-to-face molecules in the same layer (2 and 3, 0.7 - 1.0 nm). Therefore, tails with similar chemical composition from top and bottom molecular pairs will tend to aggregate together. Also, this conformation provides less crowded packing between alkyl tails.

8. Polarized light microscopy observation of crystal phases in C_{22}PhBAEO_3:

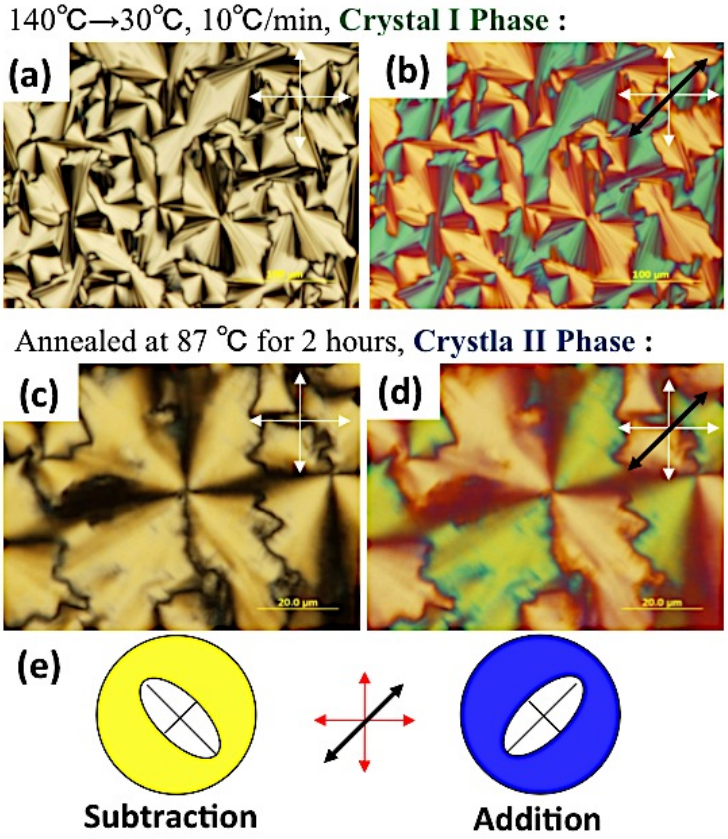

Figure S12.POM morphology of *crystal I* (a) and *crystal II* (c) phases. POM image with tint plate inserted of *crystal I* (b) and *crystal II* (d) phases. The white cross in the right top of the images indicates the polarization directions of analyzer and polarizer. The black arrow in (b), (d) and (e) indicates the slow axis of the tint plate. (e) Illustrations of the addition and subtraction effect when a tint plate is applied in the light path during POM observation. The short axis of the ellipsoid indicates the slow axis orientation of the material.

The samples prepared for POM were melt-processed between two bare cover glass slides. The samples had a typical thickness of 5 μm between the glass slides and underwent various thermal treatments before observations.

Figure S12 shows the phase morphologies of the *crystal I* and *crystal II* phases observed under POM. Both phases possessed birefringent fan shape morphology as shown in Figures S12a and S12c, respectively. After the tint plate was applied in the light path with the slow axis 45^{o} apart from the polarizer and analyzer, blue and yellow colors can be observed on the morphology. As indicated in figure S12e, when the slow axis of the plate is perpendicular to that of the material, subtraction effect occurs, and the morphology reveals a yellow color. If the slow axis of the plate is parallel to that of the material, addition effect occurs and the morphology reveals a blue color. As analyzed above, the slow axis of the columns is parallel to the column normal according to the aromatic core orientation. However, the slow axis of alkyl tail crystal, which is the *b*-axis,[10] is perpendicular to the column normal. As seen in Figure 6 in the main article, the column long axis is perpendicular to the fan shape radius directionin *crystal I* phase. Therefore, the first and third quadrant of the fan morphology revealed blue color in Figure S12b because the alkyl chain conformation was less ordered within the *crystal I* phase, and the columns dominated the displayed color. In transition to *crystal II* phase (Figure 6e & 6f in the main article), a certain ratio of columns rearranged to make their long axis parallel to the fan radius direction and the alkyl tails also rearranged within the hydrophobic layers and possessed much higher order and crystallinity. Therefore, the displayed color gradually affected by the rearranged columns and the crystals formed by alkyl tails changed from blue toward green in the first and third quadrant as shown in

Figure S12d. The POM morphology analysis has also confirmed the structure analysis results discussed in the main article.

Reference

1. E. Fernandez-Megia, J. Correa, I. Rodriguez-Meizoso and R. Riguera, *Macromolecules*, 2006, **39**, 2113-2120.
2. C. Xue, S. Jin, X. Weng, J. J. Ge, Z. Shen, H. Shen, M. J. Graham, K.-U. Jeong, H. Huang, D. Zhang, M. Guo, F. W. Harris, S. Z. D. Cheng, C. Y. Li and L. Zhu, *Chem. Mater.*, 2004, **16**, 1014-1025.
3. N. V. Venkataraman and S. Vasudevan, *J. Phys. Chem. B*, 2001, **105**, 1805-1812.
4. R. G. Synder and J. H. Shchachtschnelder, *Spectrochim. Acta*, 1963, **19**, 117-168.
5. H. Shen, K.-U. Jeong, M. Graham, S. Leng, H. Huang, B. Lotz, H. Hou, F. Harris and S. Cheng, *J. Macromol. Sci., Part B*, 2006, **45**, 215-229.
6. H. Shen, K.-U. Jeong, H. Xiong, M. J. Graham, S. Leng, J. X. Zheng, H. Huang, M. Guo, F. W. Harris and S. Z. D. Cheng, *Soft Matter*, 2006, **2**, 232.
7. G. Ungar, *J. Phys. Chem.*, 1983, **87**, 689-695.
8. G. Ungar, *Macromolecules*, 1986, **19**, 1317-1324.
9. G. Ungar and N. Masic, *J. Phys. Chem.*, 1985, **89**, 1036-1042.
10. M. S. Kim and K. Levon, *Eur. Polym. J.*, 1997, **33**, 1787-1798.